

Structural transfer learning of non-Gaussian DAG

Mingyang Ren¹, Xin He² and Junhui Wang¹

¹Department of Statistics, The Chinese University of Hong Kong

²School of Statistics and Management,
Shanghai University of Finance and Economics

Abstract

Directed acyclic graph (DAG) has been widely employed to represent directional relationships among a set of collected nodes. Yet, the available data in one single study is often limited for accurate DAG reconstruction, whereas heterogeneous data may be collected from multiple relevant studies. It remains an open question how to pool the heterogeneous data together for better DAG structure reconstruction in the target study. In this paper, we first introduce a novel set of structural similarity measures for DAG and then present a transfer DAG learning framework by effectively leveraging information from auxiliary DAGs of different levels of similarities. Our theoretical analysis shows substantial improvement in terms of DAG reconstruction in the target study, even when no auxiliary DAG is overall similar to the target DAG, which is in sharp contrast to most existing transfer learning methods. The advantage of the proposed transfer DAG learning is also supported by extensive numerical experiments on both synthetic data and multi-site brain functional connectivity network data.

Keywords: Directed acyclic graph, heterogeneous data, structural equation model, structural similarity, topological layer

1 Introduction

Directed acyclic graph (DAG) provides an efficient tool to represent directed relationships among a set of random variables, which has been widely employed in various application domains, ranging from biomedicine, economics, to psychology. It has also attracted tremendous interest from researchers, and various DAG learning algorithms have been proposed,

including Chen et al. (2019), Yuan et al. (2019) and Park (2020), on Gaussian DAG with equal noise variance (Peters and Bühlmann, 2014). The pioneering work of Shimizu et al. (2006) unveiled the research route on non-Gaussian DAG, which has received increasing attention in recent years (Hyvärinen and Smith, 2013; Wang and Drton, 2020; Zhao et al., 2022).

Despite their successes, existing DAG learning methods have mainly focused on a dataset from one single study, whose sample size can be extremely limited due to the rarity of certain diseases and the high acquisition costs in many biomedical applications. Nonetheless, fast-growing academic cooperation makes it possible for relevant data collected at other research institutions to contribute to a given target institution. As the motivating example, our analysis goal is to construct directed brain networks of attention deficit hyperactivity disorder (ADHD) patients based on brain image data from different sites, whose sample sizes vary from tens to hundreds. To fully utilize the heterogeneous data from different sites, transfer learning, aiming at transferring the information from auxiliary domains to improve learning performance on the target domain, is a promising solution with gaining attention.

Transfer learning has been extensively investigated in the machine learning community; interested readers may refer to Zhuang et al. (2020) and the references therein. Yet, most existing transfer learning methods are algorithm-based, and the statistical guarantees of transfer learning still remain insufficient and grow in popularity. Particularly, Cai and Wei (2021); Reeve et al. (2021) proposed some minimax and adaptive transfer learning-based classifiers. Li et al. (2022a) proposed a transfer learning method for high-dimensional linear regression models with minimax optimality, which is extended to high-dimensional generalized linear regression models (Tian and Feng, 2022; Li et al., 2023a) and federated learning (Li et al., 2023b). In contrast, transfer learning for unsupervised learning is in its infancy (Li et al., 2022b), and largely follows the idea of parameter transfer as for supervised learning. Another closely related but rather different topic is multi-task DAG learning, which

estimates the same DAG shared by multiple datasets (Danks et al., 2008; Triantafillou and Tsamardinos, 2015; Mooij et al., 2020; Huang et al., 2020), or multiple different DAGs with certain structural similarities (Shimizu, 2012; Liu et al., 2019; Wang et al., 2020; Chen et al., 2021).

There are at least two outstanding challenges for transfer DAG learning that cannot be properly addressed by directly extending the existing transfer learning methods. First, compared with parameter estimation, a more important task in transfer DAG learning is to recover its graph structure by transferring structural knowledge from auxiliary domains. *Structure transfer* is substantially different from *parameter transfer*, which requires appropriate measures of structural similarity between DAGs, globally or locally. Second, *global or overall similarity* is a widely adopted assumption in the existing literature of transfer learning, which assures that all parameters of an informative auxiliary domain are close to those of the target domain as a whole. For DAGs, this overall similarity would require the whole structure of an auxiliary DAG to be similar to that of the target DAG, which is often too ideal in practice. Therefore, how auxiliary DAGs with *local similarity* can help with DAG learning through *structure transfer* remains a challenging open question.

In this article, in addition to parametric similarity, we propose a novel set of structural similarity measures for auxiliary and target DAGs, from global-level, layer-level to node-level. Then, focusing on linear non-Gaussian DAGs, we further propose a transfer DAG learning framework, which can detect structure-informative auxiliary DAGs benefiting from the well-defined structural similarity measures, and the topological layers of the target DAG can be better recovered with the help of the detected auxiliary DAGs. The theoretical and numerical improvements of the proposed transfer DAG learning framework compared with its single-task learning alternatives are also investigated.

Main contributions of the proposed framework are multi-fold. First, a novel set of DAG structural similarity measures with different levels are proposed, which are the progressive

and comprehensive definition development from global and macroscopic to local and micro-cosmic. Such structural similarity measures constitute a fundamental complement to the parametric similarity in transfer learning. Second, a transfer DAG learning framework is developed accordingly, which accommodates auxiliary DAGs with different levels of structural similarities, achieving both *structure transfer* and *parameter transfer*. In the realistic case where the structure-informative auxiliary DAGs are only locally similar to the target DAG on some nodes, structure transfer with only local similarity is an important extension of the existing parameter transfer paradigm requiring global or overall similarity. Third, the theoretical analysis shows that the proposed transfer DAG learning is advantageous in terms of DAG reconstruction of the target domain even in high-dimensional settings, including more relaxed conditions, reduced probability of failure in topology layer reconstruction and target sample complexity, and improved estimation. Last but not least, the proposed transfer DAG learning is applied on the ADHD brain functional connectivity analysis, which goes beyond the common undirected brain network analysis and provides some interesting neurophysiological insights into the pathogenesis from the directed regulatory relationships between brain regions.

The rest of the paper is organized as follows. Section 2 introduces the necessary notations and backgrounds of DAGs. Section 3 presents the novel set of DAG similarity measures. Sections 4 and 5 introduce the proposed transfer DAG learning framework and establish its DAG reconstruction consistency. Numerical experiments on the synthetic dataset and the multi-site ADHD brain connectivity network data are conducted in Sections 6 and 7, respectively. A brief discussion is contained in Section 8, and all technical proofs and additional numerical results are provided in the Supplementary File.

2 Preliminaries

This section introduces some necessary notations and basic concepts of DAG that will be used throughout the paper.

2.1 Notations

Denote $\|\mathbf{u}\|_q$ as the l_q -norm of a vector \mathbf{u} , for $q \geq 0$. For a matrix $\mathbf{A} = (A_{ij})_{1 \leq i, j \leq p}$, let \mathbf{A}_j be its j -th column and \mathbf{A}_{-jj} be the \mathbf{A}_j without θ_{jj} , $\|\mathbf{A}\|_{q, \infty} = \max_{1 \leq j \leq p} \|\mathbf{A}_j\|_q$, $\|\mathbf{A}\|_1 = \sum_{j=1}^p \|\mathbf{A}_j\|_1$, $\|\mathbf{A}\|_{\max} = \max_{1 \leq i, j \leq p} |A_{ij}|$, $\|\mathbf{A}\|_{1, \text{off}} = \sum_{1 \leq i \neq j \leq p} |A_{ij}|$, and $\|\mathbf{A}\|_F$ be the Frobenius norm of \mathbf{A} . When \mathbf{A} is symmetric, we further denote $\psi_{\min}(\mathbf{A})$ and $\psi_{\max}(\mathbf{A})$ as the smallest and largest eigenvalues of \mathbf{A} , respectively. Let \mathbf{A}_S be the submatrix of \mathbf{A} labeled by S . Let $|S|$ be the cardinality of a set S and $[K] = \{1, \dots, K\}$ be the K -set for any positive integer K . For sequences a_n and b_n , define $a_n \lesssim b_n$ if there exists a positive constant C such that $a_n \leq Cb_n$, and $a_n \asymp b_n$ if $a_n \lesssim b_n$ and $b_n \lesssim a_n$. For two real numbers a and b , define $a \wedge b = \min\{a, b\}$ and $a \vee b = \max\{a, b\}$. The superscript $*$ on a parameter marks its true value.

2.2 DAG and topological layers

Consider a DAG $\mathcal{G} = \{\mathcal{N}, \mathcal{E}\}$, encoding the joint distribution $P(\mathbf{x})$ of $\mathbf{x} = (x_1, \dots, x_p)^T \in \mathbb{R}^p$, where $\mathcal{N} = \{1, \dots, p\}$ consists of a set of nodes associated with each coordinate of \mathbf{x} , and $\mathcal{E} \subset \mathcal{N} \times \mathcal{N}$ consists of all the directed edges among the nodes. For each node j , its parents, children, and descendants are denoted as pa_j , ch_j , and de_j , respectively. Each node x_j is also centered with mean zero.

Suppose that the joint distribution of \mathbf{x} can also be embedded into a linear structural

equation model (SEM),

$$x_j = \sum_{l \in \text{pa}_j} \beta_{jl} x_l + \epsilon_j; \quad j = 1, \dots, p, \quad (2.1)$$

where $\beta_{jl} \neq 0$ for any $l \in \text{pa}_j$, ϵ_j denotes a continuous *non-Gaussian* noise with variance σ_j^2 , and $\epsilon_l \perp\!\!\!\perp \epsilon_j$ for any $l \neq j$. This independent noise condition also implies that $\epsilon_j \perp\!\!\!\perp x_l$ for any $l \notin \text{de}_j \cup \{j\}$. It is commonly assumed that there is no unobserved confounding effect among the observed nodes in \mathcal{G} (Spirtes et al., 2000). Furthermore, the SEM model in (2.1) can be rewritten as a matrix form $\mathbf{x} = \mathbf{B}\mathbf{x} + \boldsymbol{\epsilon}$ with $\mathbf{B} = (\beta_{jl})_{j,l} \in \mathbb{R}^{p \times p}$ and $\boldsymbol{\epsilon} = (\epsilon_1, \dots, \epsilon_p)^\top$ is the noise vector with covariance matrix $\boldsymbol{\Omega} = \text{diag}\{\sigma_1^2, \dots, \sigma_p^2\}$. It follows that

$$\mathbf{x} = (\mathbf{I} - \mathbf{B})^{-1} \boldsymbol{\epsilon} = \mathbf{A} \boldsymbol{\epsilon}, \quad (2.2)$$

and $x_j = \sum_{l=1}^p a_{jl} \epsilon_l$, where a_{jl} is the (j, l) -th element of $\mathbf{A} = (\mathbf{I} - \mathbf{B})^{-1}$, representing the total effect of x_l on x_j . The SEM model implies that $\epsilon_l \perp\!\!\!\perp x_j$ and thus $a_{jl} = 0$ for any node $l \in \text{de}_j$. Moreover, the covariance matrix of \mathbf{x} is $\boldsymbol{\Sigma} = (\mathbf{I} - \mathbf{B})^{-1} \boldsymbol{\Omega} (\mathbf{I} - \mathbf{B})^{-T}$, and the corresponding precision matrix is $\boldsymbol{\Theta} = \boldsymbol{\Sigma}^{-1} = (\mathbf{I} - \mathbf{B})^\top \boldsymbol{\Omega}^{-1} (\mathbf{I} - \mathbf{B})$. We remark that non-Gaussian DAGs do not require equal or ordered noise variance conditions to ensure identifiability, which is necessary for Gaussian DAGs (Peters and Bühlmann, 2014; Ghoshal and Honorio, 2018) and may parameterize structural information.

Without loss of generality, assume \mathcal{G} has a total of T topological layers (Zhao et al., 2022). All the leaf nodes and isolated nodes in \mathcal{G} belong to the lowest layer \mathcal{A}_0 . For $t = 1, \dots, T-1$, \mathcal{A}_t denotes all the nodes contained in the t -th layer, whose longest distance to a leaf node is exactly t . It is then clear that $\cup_{t=0}^{T-1} \mathcal{A}_t = \mathcal{N}$. Further, for each node $j \in \mathcal{A}_t$, it follows from the layer construction that $\text{pa}_j \subset \mathcal{S}_{t+1} = \cup_{d=t+1}^{T-1} \mathcal{A}_d$, and $\mathcal{S}_0 = \mathcal{N}$. Therefore, acyclicity is automatically guaranteed. Denote $\boldsymbol{\Theta}^{\mathcal{S}_t}$ and $\boldsymbol{\Sigma}_{\mathcal{S}_t}$ as the precision and covariance matrices of

$\mathbf{x}_{\mathcal{S}_t}$, respectively. Note that the submatrix of the precision matrix $\Theta_{\mathcal{S}_t} \neq \Theta^{\mathcal{S}_t}$ and $\Theta^{\mathcal{S}_0} = \Theta$. The topological layers can help reconstruct the DAG structure. Particularly, for any $j \in \mathcal{S}_t$, regressing x_j on $\mathbf{x}_{\mathcal{S}_t \setminus \{j\}}$ yields the expected residual $e_{j,\mathcal{S}_t} = x_j + \mathbf{x}_{\mathcal{S}_t \setminus \{j\}}^\top [\Theta^{\mathcal{S}_t}]_{-jj} / [\Theta^{\mathcal{S}_t}]_{jj}$. It was shown in Zhao et al. (2022) that

$$j \in \mathcal{A}_t \text{ if and only if } e_{j,\mathcal{S}_t} \perp\!\!\!\perp x_l \text{ for any } l \in \mathcal{S}_t \setminus \{j\}. \quad (2.3)$$

This result leads to a simple bottom-up learning algorithm to re-construct \mathcal{A}_t for $t = 0, 1, \dots, T-1$ by using the independence test. More importantly, this layer reconstruction algorithm also motivates us to design new concepts and methods for transfer learning of DAG accordingly.

3 DAG similarity measures

Denote the target DAG as $\mathcal{G}_0 = \{\mathcal{N}, \mathcal{E}_0\}$, which encodes the joint distribution $P_0(\mathbf{x})$ of $\mathbf{x} = (x_1, \dots, x_p)^T$ with the precision matrix Θ . Suppose that there also exist K auxiliary DAGs $\mathcal{G}_k = \{\mathcal{N}, \mathcal{E}_k\}$ with $k \in [K]$, encoding the joint distribution $P_k(\mathbf{x}^{(k)})$ of $\mathbf{x}^{(k)} = (x_1^{(k)}, \dots, x_p^{(k)})^T$ with the precision matrix $\Theta^{(k)}$ and the covariance matrix $\Sigma^{(k)}$. The auxiliary domain k can also be embedded into a linear SEM (2.1) with different parameters including the continuous non-Gaussian noise $\epsilon_j^{(k)}$ and its variance $[\sigma_j^{(k)}]^2$. It is of great interest to improve the learning accuracy of \mathcal{G}_0 in the target domain by leveraging information from \mathcal{G}_k in the auxiliary domains.

The effectiveness of such a transfer learning task is heavily based on measuring the similarity between \mathcal{G}_0 and \mathcal{G}_k . In particular, we propose two similarity measures for DAG, corresponding to the strength or presence of causal effects between nodes in different domains as measured in the parameters or graph structures. Denote the divergence matrix as $\Delta_{\mathcal{S}_t}^{(k)} =$

$\Theta^{\mathcal{S}_t} \Sigma_{\mathcal{S}_t}^{(k)} - \mathbf{I}_{|\mathcal{S}_t|}$, where $\mathbf{I}_{|\mathcal{S}_t|}$ is the $|\mathcal{S}_t|$ -dimensional identity matrix. It measures the similarity between the precision matrices regarding the t -th layer in the target and the k -th auxiliary domains. By using $\Delta_{\mathcal{S}_t}^{(k)}$, Definition 1 defines a parametric similarity between \mathcal{G}_0 and \mathcal{G}_k .

Definition 1. (*Parametric Similarity*) \mathcal{G}_k is layer- t parameter-informative, if $\|\Delta_{\mathcal{S}_t}^{(k)}\|_{1,\infty} + \|(\Delta_{\mathcal{S}_t}^{(k)})^\top\|_{1,\infty} \leq h_t$ for some small $h_t > 0$.

It is clear that a small value of h_t indicates the precision matrices corresponding to \mathcal{S}_t in the target and auxiliary domains are close, and thus the information from the auxiliary domain can help improve the estimation accuracy of Θ in the target domain. Definition 1 is reminiscent of the overall similarity in literature (Li et al., 2022b), but parametric similarity in Θ does not necessarily imply similar DAG structures. Figure 1 gives a toy example, where the DAGs in (a) and (b) are parametric similar, provided that the three red directed edges in (b) are of weak strength. Yet, the graph structures and topological layers in (a) and (b) are substantially different, and thus additional structural similarity is necessary to quantify similarity between DAGs.

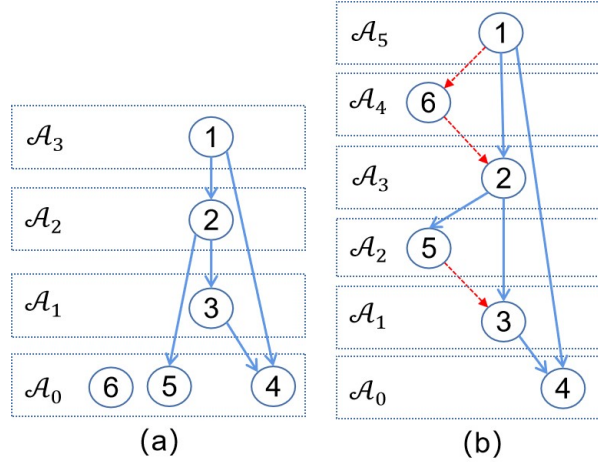


Figure 1: Some toy examples for DAGs with parametric similarity but no structural similarity.

Definition 2 is among the first attempts to provide some well-defined and comprehensive

structural similarities between DAGs, which take advantage of the topological layers and shall greatly facilitate transfer learning for DAGs in various scenarios.

Definition 2. (*Structural Similarity*)

- (a) \mathcal{G}_k is global structure-informative, if it has the same number of layers as \mathcal{G}_0 , and $\mathcal{A}_t = \mathcal{A}_t^{(k)}$ for any $t = 0, 1, \dots, T-1$, where \mathcal{A}_t and $\mathcal{A}_t^{(k)}$ are the nodes contained in the t -th layers of \mathcal{G}_0 and \mathcal{G}_k , respectively.
- (b) \mathcal{G}_k is layer- t structure-informative, if for some $t \in \{0, 1, \dots, T-1\}$, there exists $t' \geq 0$, such that $\mathcal{A}_t = \mathcal{A}_{t'}^{(k)}$ and $\mathcal{S}_t = \mathcal{S}_{t'}^{(k)}$.
- (c) \mathcal{G}_k is node- j structure-informative, if (i) $de_j^{(k)} \cap \mathcal{S}_{t_j} = \emptyset$ and (ii) $de_j^{(k)} \cap \mathcal{A}_{t_j-1} \neq \emptyset$ with $t_j \geq 1$, where t_j denotes the layer to which node- j belongs in \mathcal{G}_0 , and $de_j^{(k)}$ denotes node j 's descendants in \mathcal{G}_k .

From Definition 2a, a global structure-informative DAG needs to have exactly the same topological layers as the target DAG. It is important to remark that the global structural similarity concerns only the membership of nodes in each topological layer, and does not impose any requirements on edges between nodes in different layers. The layer-level structural similarity in Definition 2b focuses on the relative positions of one particular topological layer in \mathcal{G}_0 and \mathcal{G}_k . This similarity ensures that information from \mathcal{G}_k can be efficiently transferred when constructing the topological layer of interest in \mathcal{G}_0 . The node-level structural similarity in Definition 2c is a very weak requirement, focusing on local and microcosmic structures of DAGs. A node- j structure-informative DAG only shares a similar relative position of node j as \mathcal{G}_0 , where the relative position can be depicted in two cases. Case (i) requires no overlap between node j 's descendants in \mathcal{G}_k and \mathcal{S}_{t_j} in \mathcal{G}_0 , and thus information from \mathcal{G}_k can prevent assigning node j to a topological layer higher than t_j in \mathcal{G}_0 . Case (ii) requires node j 's descendants in \mathcal{G}_k overlap with \mathcal{A}_{t_j-1} in \mathcal{G}_0 , which can prevent assigning node j to

a topological layer lower than t_j in \mathcal{G}_0 . It can be verified that these three levels of structural similarities are progressive; that is, a global structure-informative DAG must be layer- t structure-informative for all layers, and a layer- t structure-informative DAG must be node- j structure-informative for all nodes in \mathcal{A}_t . For illustration, Figure 2 gives some toy examples of these three structural similarities, where only two auxiliary DAGs are informative while others can be of arbitrary structure and thus non-informative.

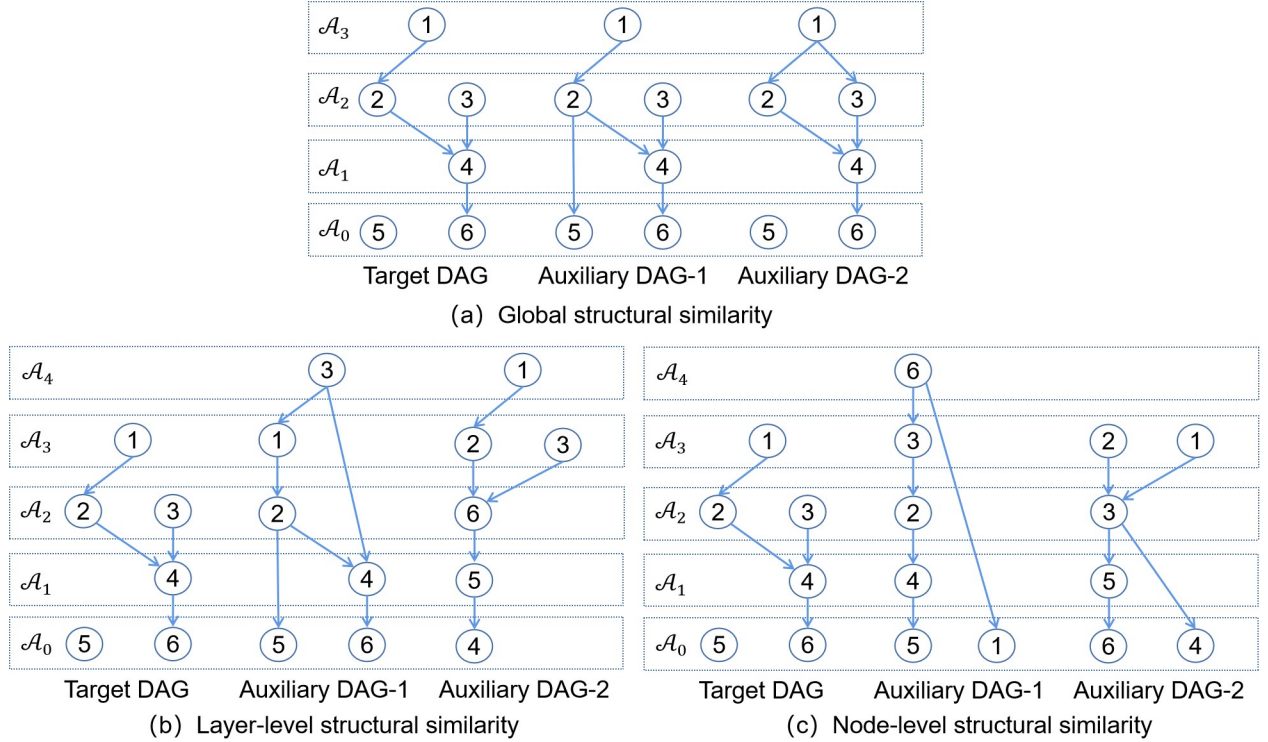


Figure 2: Some toy examples for DAGs in the target and auxiliary domains with different levels of structural similarities.

It can be observed in Figure 2a that both \mathcal{G}_1 and \mathcal{G}_2 are global structure-informative, which have the same topological layers as \mathcal{G}_0 but their directed edge sets are all different. In Figure 2b, \mathcal{G}_1 is layer-0 and layer-1 structure-informative, and \mathcal{G}_2 is layer-2 and layer-3 structure-informative. They share the same nodes in the respective layers as \mathcal{G}_0 , but the composition of other layers is largely different. In Figure 2c, \mathcal{G}_1 is node-2, node-4, and node-5 structure-informative, and \mathcal{G}_2 are node-1, node-3, and node-6 structure-informative. Take

node-2 as an example, when constructing layer \mathcal{A}_1 of \mathcal{G}_0 , \mathcal{G}_1 provides useful information to prevent mis-assigning node 2 to \mathcal{A}_1 , since node 4 is a child of node 2 in \mathcal{G}_1 and belongs to \mathcal{A}_1 of \mathcal{G}_0 . On the other hand, when constructing \mathcal{A}_2 of \mathcal{G}_0 after \mathcal{A}_0 and \mathcal{A}_1 are determined, \mathcal{G}_1 provides information to assign node 2 to \mathcal{A}_2 , thanks to the fact that node 2's descendants in \mathcal{G}_1 do not appear in \mathcal{S}_2 of \mathcal{G}_0 . Similar observations can also be made for other nodes.

4 Transfer DAG learning

Suppose in addition to $\mathbf{X} = (\mathbf{x}_1, \dots, \mathbf{x}_p) \in \mathbb{R}^{n \times p}$ with $\mathbf{x}_j = (x_{1j}, \dots, x_{nj})^\top$ from the target domain with \mathcal{G}_0 , we also observe $\{\mathbf{X}^{(k)}\}_{k=1}^K$ from K auxiliary domains with $\mathbf{X}^{(k)} \in \mathbb{R}^{n_k \times p}$, where n and n_k are sample sizes of the target and the k -th auxiliary domains, respectively, and $n \lesssim n_k$ for any $k \in [K]$. The primary goal is to leverage information in $\{\mathbf{X}^{(k)}\}_{k=1}^K$ to help construct \mathcal{G}_0 .

The proposed generic transfer DAG learning framework is summarized in Algorithm 1, where \mathcal{A}_t 's are first constructed in a bottom-up fashion from $t = 0$ to $t = T - 1$ by leveraging the detected informative auxiliary DAGs with various structural similarities, and then directed edges are determined between nodes in different layers based on the estimated target precision matrix.

In Step 2a of Algorithm 1, the distance covariance and its related independence test (Székely et al., 2007) are employed. To be self-contained, we briefly restate its definition here. Given $\widehat{\mathcal{S}}_t \subseteq \{1, \dots, p\}$, the distance covariance between the expected residual $e_{j, \widehat{\mathcal{S}}_t}$ and the variable x_l is defined as $\text{dcov}^2(e_{j, \widehat{\mathcal{S}}_t}, x_l) = I_{jtl,1} + I_{jtl,2} - 2I_{jtl,3}$, where $I_{jtl,1} = E[|e_{j, \widehat{\mathcal{S}}_t} - e'_{j, \widehat{\mathcal{S}}_t}| |x_l - x'_l|]$, $I_{jtl,2} = E[|e_{j, \widehat{\mathcal{S}}_t} - e'_{j, \widehat{\mathcal{S}}_t}|] E[|x_l - x'_l|]$ and $I_{jtl,3} = E(E[|e_{j, \widehat{\mathcal{S}}_t} - e'_{j, \widehat{\mathcal{S}}_t}| |e_{j, \widehat{\mathcal{S}}_t}]) E[|x_l - x'_l| |x_l|]$ with $e'_{j, \widehat{\mathcal{S}}_t}$ and x'_l denoting an independent copy of $e_{j, \widehat{\mathcal{S}}_t}$ and x_l , respectively. It provides a neat independence criterion in that $\text{dcov}^2(e_{j, \widehat{\mathcal{S}}_t}, x_l) = 0$ if $e_{j, \widehat{\mathcal{S}}_t} \perp\!\!\!\perp x_l$ and $\text{dcov}^2(e_{j, \widehat{\mathcal{S}}_t}, x_l) > 0$

Algorithm 1 Transfer DAG learning framework

- 1: **Input:** \mathbf{X} , $\{\mathbf{X}^{(k)}\}_{k=1}^K$, $\widehat{\mathcal{S}}_t = \{1, \dots, p\}$, $\widehat{\mathbf{B}} = \{\hat{\beta}_{ij}\}_{i,j=1}^p = \mathbf{0}_{p \times p}$, and $t = 0$.
 - 2: **Repeat:** until $|\widehat{\mathcal{S}}_t| \leq 1$:
 - (a) Construct $\widehat{\mathcal{A}}_t$ via independence test leveraging the detected informative auxiliary domains;
 - (b) Estimate $\widehat{\text{pa}}_j = \{l \in \widehat{\mathcal{S}}_t \setminus \widehat{\mathcal{A}}_t : [\widehat{\boldsymbol{\Theta}}^{\widehat{\mathcal{S}}_t}]_{jl} \neq 0\}$ and $\hat{\beta}_{jl} = -[\widehat{\boldsymbol{\Theta}}^{\widehat{\mathcal{S}}_t}]_{jl}/[\widehat{\boldsymbol{\Theta}}^{\widehat{\mathcal{S}}_t}]_{jj}$ for any $j \in \widehat{\mathcal{A}}_t$ and $l \in \widehat{\text{pa}}_j$;
 - (c) Update $\widehat{\mathcal{S}}_{t+1} \leftarrow \widehat{\mathcal{S}}_t \setminus \widehat{\mathcal{A}}_t$ and $t \leftarrow t + 1$.
 - 3: If $|\widehat{\mathcal{S}}_t| = 1$, set $\widehat{T} = t + 1$ and $\widehat{\mathcal{A}}_t = \widehat{\mathcal{S}}_t$; otherwise set $\widehat{T} = t$.
 - 4: **Return:** $\{\widehat{\mathcal{A}}_t\}_{t=0}^{\widehat{T}-1}$ and $\widehat{\mathbf{B}}$.
-

otherwise. On the target domain, an empirical version of $\text{dcov}^2(e_{j,\widehat{\mathcal{S}}_t}, x_l)$ is

$$\widehat{\text{dcov}}^2(\widehat{e}_{j,\widehat{\mathcal{S}}_t}, \mathbf{x}_l) = \widetilde{I}_{jtl,1} + \widetilde{I}_{jtl,2} - 2\widetilde{I}_{jtl,3}, \quad (4.1)$$

where $\widehat{e}_{j,\widehat{\mathcal{S}}_t} = \mathbf{X}_{\widehat{\mathcal{S}}_t}[\widehat{\boldsymbol{\Theta}}^{\widehat{\mathcal{S}}_t}]_{\cdot j}/[\widehat{\boldsymbol{\Theta}}^{\widehat{\mathcal{S}}_t}]_{jj} = (\widehat{e}_{1j,\widehat{\mathcal{S}}_t}, \dots, \widehat{e}_{nj,\widehat{\mathcal{S}}_t})^\top$, $\widetilde{I}_{jtl,1} = \frac{1}{n^2} \sum_{i,i'=1}^n |\widehat{e}_{ij,\widehat{\mathcal{S}}_t} - \widehat{e}_{i'j,\widehat{\mathcal{S}}_t}| |x_{il} - x_{i'l}|$, $\widetilde{I}_{jtl,2} = (\frac{1}{n^2} \sum_{i,i'=1}^n |\widehat{e}_{ij,\widehat{\mathcal{S}}_t} - \widehat{e}_{i'j,\widehat{\mathcal{S}}_t}|)(\frac{1}{n^2} \sum_{i,i'} |x_{il} - x_{i'l}|)$, and $\widetilde{I}_{jtl,3} = \frac{1}{n^3} \sum_{i,i',h=1}^n |\widehat{e}_{ij,\widehat{\mathcal{S}}_t} - \widehat{e}_{hj,\widehat{\mathcal{S}}_t}| |x_{i'l} - x_{hl}|$. It can be employed to test $\mathcal{H}_0 : e_{j,\widehat{\mathcal{S}}_t} \perp\!\!\!\perp x_l$ vs $\mathcal{H}_1 : e_{j,\widehat{\mathcal{S}}_t} \not\perp\!\!\!\perp x_l$ with test statistic

$$\widehat{T}(\widehat{e}_{j,\widehat{\mathcal{S}}_t}, \mathbf{x}_l) = \widehat{\text{dcov}}^2(\widehat{e}_{j,\widehat{\mathcal{S}}_t}, \mathbf{x}_l) / \widetilde{I}_{jtl,2}.$$

Specifically, \mathcal{H}_0 is rejected if $n\widehat{T}(\widehat{e}_{j,\widehat{\mathcal{S}}_t}, \mathbf{x}_l) > (\Phi^{-1}(1 - \alpha/2))^2$, where $\Phi(\cdot)$ denotes the distribution function of standard normal distribution, and α is the significance level. Furthermore, on the k -th auxiliary domain, $\widehat{\text{dcov}}^2(\widehat{e}_{j,\widehat{\mathcal{S}}_t}^{(k)}, \mathbf{x}_l^{(k)})$ and $\widehat{T}(\widehat{e}_{j,\widehat{\mathcal{S}}_t}^{(k)}, \mathbf{x}_l^{(k)})$ can be similarly defined by replacing $\mathbf{X}_{\widehat{\mathcal{S}}_t}$ and $\widehat{\boldsymbol{\Theta}}^{\widehat{\mathcal{S}}_t}$ with $\mathbf{X}_{\widehat{\mathcal{S}}_t}^{(k)}$ and $(\widehat{\boldsymbol{\Theta}}^{(k)})^{\widehat{\mathcal{S}}_t}$, respectively.

It is clear that a key to transfer DAG learning is to obtain $\widehat{\mathcal{A}}_t$ based on the detected auxiliary domains with various structural similarities. We begin with a naive case where a globally informative \mathcal{G}_k is available, and then a more realistic case with only node-level structure-informative \mathcal{G}_k . The case with layer-level structure-informative \mathcal{G}_k 's can be treated

in a similar way and thus omitted.

4.1 Global structural transfer in naive case

We first consider a naive case with an ideal auxiliary DAG \mathcal{G}_k , which is both parameter-informative and global structure-informative. It shares the same topological layers and similar parameters with \mathcal{G}_0 , and thus can provide full information for its reconstruction. This naive case is reminiscent of the overall similarity in the existing literature on transfer learning (Li et al., 2022b,a; Tian and Feng, 2022) and multi-task learning (Huang et al., 2020; Chen et al., 2021), which can serve as a benchmark for the local structural transfer in Section 4.2.

We detect this ideal auxiliary DAG as

$$\check{k} = \underset{k \in [K]}{\operatorname{argmin}} \left(\|\widehat{\Delta}^{(k)}\|_{1,\infty} + \|(\widehat{\Delta}^{(k)})^\top\|_{1,\infty} \right), \quad (4.2)$$

with the divergence matrix $\widehat{\Delta}^{(k)} = \widehat{\Theta}^{(0)} \widehat{\Sigma}^{(k)} - \mathbf{I}_p$, where $\widehat{\Theta}^{(0)}$ is an initial estimate based on the target samples \mathbf{X} only. Once \check{k} is detected, $\widehat{\mathcal{A}}_t$ can be obtained by testing independence between $\widehat{\mathbf{e}}_{j,\widehat{\mathcal{S}}_t}^{(\check{k})}$ and $\{\mathbf{x}_l^{(\check{k})} : l \in \widehat{\mathcal{S}}_t \setminus \{j\}\}$ for each node j based on distance covariance,

$$\widehat{\mathcal{A}}_t = \left\{ j : \max_{l \in \widehat{\mathcal{S}}_t \setminus \{j\}} n_{\check{k}} \widehat{T}(\widehat{\mathbf{e}}_{j,\widehat{\mathcal{S}}_t}^{(\check{k})}, \mathbf{x}_l^{(\check{k})}) \leq (\Phi^{-1}(1 - \alpha_{\check{k}}/2))^2 \right\}, \quad (4.3)$$

where $\alpha_{\check{k}}$ is the significance level of the independence test, and $\widehat{\mathbf{e}}_{j,\widehat{\mathcal{S}}_t}^{(\check{k})}$ can be obtained based on $(\widehat{\Theta}^{(\check{k})})^{\widehat{\mathcal{S}}_t}$. It is clear that (4.3) is solely based on $\mathcal{G}_{\check{k}}$, which shares exactly the same topological layers as \mathcal{G}_0 and thus is able to accurately determine the nodes in each \mathcal{A}_t .

The global structure transfer learning for DAG largely relies on the existence of an ideal auxiliary DAG, which, unfortunately, can be rare in practice. If this ideal auxiliary DAG does not exist, the performance of the global structure transfer learning can be even deteriorated

due to inappropriate information transfer. Such an undesirable effect is also known as “negative transfer” in the literature (Li et al., 2022b,a; Tian and Feng, 2022), which raises demands for more robust local transfer methods.

4.2 Local structural transfer in more realistic case

We now turn to a more realistic case where no auxiliary DAG is global structure-informative, but node-level structure-informative DAGs satisfying Definition 2c for each node are present. We then need to detect node-level structure-informative auxiliary DAGs for each node one by one, so that \mathcal{G}_0 can still be reconstructed.

To capture the local similarity with respect to node j , we introduce a novel index to detect the most informative auxiliary DAG. Specifically, for any node $j \in \widehat{\mathcal{S}}_t$, we set

$$k_{j,t}^{no} = \operatorname{argmin}_{k \in [K]} \left| \max_{l \in \widehat{\mathcal{S}}_t \setminus \{j\}} \widehat{\operatorname{dcov}}^2(\widehat{\mathbf{e}}_{j,\widehat{\mathcal{S}}_t}, \mathbf{x}_l) - \max_{l' \in \widehat{\mathcal{S}}_t \setminus \{j\}} \widehat{\operatorname{dcov}}^2(\widehat{\mathbf{e}}_{j,\widehat{\mathcal{S}}_t}^{(k)}, \mathbf{x}_{l'}^{(k)}) \right|, \quad (4.4)$$

which is to find the auxiliary domain whose value of $\max_{l' \in \widehat{\mathcal{S}}_t \setminus \{j\}} \widehat{\operatorname{dcov}}^2(\widehat{\mathbf{e}}_{j,\widehat{\mathcal{S}}_t}^{(k)}, \mathbf{x}_{l'}^{(k)})$ is the closest to that on the target domain. The selection step in (4.4) is conducted for every node in $\widehat{\mathcal{S}}_t$. Also, the selected auxiliary DAGs for the same node can be different when constructing different topological layers, due to their different relative positions in different topological layers.

The selection criterion in (4.4) is motivated from some key observations. On one hand, we have $\max_{l \in \mathcal{S}_t \setminus \{j\}} \operatorname{dcov}^2(e_{j,\mathcal{S}_t}, x_l) = 0$ for any node $j \in \mathcal{A}_t$. If \mathcal{G}_k is node- j structure-informative, then $\max_{l' \in \mathcal{S}_t \setminus \{j\}} \operatorname{dcov}^2(e_{j,\mathcal{S}_t}^{(k)}, x_{l'}^{(k)}) = 0$. Yet, for any other non-informative $\mathcal{G}_{\tilde{k}}$ that does not satisfy Definition 2c(i), $\max_{l' \in \mathcal{S}_t \setminus \{j\}} \operatorname{dcov}^2(e_{j,\mathcal{S}_t}^{(\tilde{k})}, x_{l'}^{(\tilde{k})})$ shall be substantially away from 0. Therefore, the minimization task in (4.4) must select a node- j structure-informative auxiliary domain under Definition 2c(i). On the other hand, $\max_{l \in \mathcal{S}_t \setminus \{j\}} \operatorname{dcov}^2(e_{j,\mathcal{S}_t}, x_l)$ is substantially away from 0 for any node $j \in \mathcal{S}_t \setminus \mathcal{A}_t$. Therefore, the minimization task in (4.4)

must not select any non-informative \mathcal{G}_k with $\max_{l' \in \mathcal{S}_t \setminus \{j\}} \text{dcov}^2(e_{j, \mathcal{S}_t}^{(k)}, x_{l'}^{(k)}) = 0$.

Remark 1. Note that estimating $\hat{e}_{j, \hat{\mathcal{S}}_t}$ in (4.4) relies on $\hat{\Theta}^{\hat{\mathcal{S}}_t}$, and so does estimating both \hat{p}_{a_j} and $\hat{\beta}_{j_l}$ in Step 2b. Instead of using only the target domain, we suggest a multi-step transfer learning method to improve to estimation accuracy of $\hat{\Theta}^{\hat{\mathcal{S}}_t}$, which is applicable to any $\hat{\mathcal{S}}_t \subseteq \{1, \dots, p\}$. First, the most parameter-informative auxiliary domain is selected as $\check{k}_t = \arg\min_{k \in [K]} (\|\hat{\Delta}_t^{(k)}\|_{1, \infty} + \|(\hat{\Delta}_t^{(k)})^\top\|_{1, \infty})$ with the divergence matrix $\hat{\Delta}_t^{(k)} = (\hat{\Theta}^{\hat{\mathcal{S}}_t})^{(0)} \hat{\Sigma}_{\hat{\mathcal{S}}_t}^{(k)} - \mathbf{I}_{|\hat{\mathcal{S}}_t|}$ and an initial estimate $(\hat{\Theta}^{\hat{\mathcal{S}}_t})^{(0)}$ based only on the target samples $\mathbf{X}_{\hat{\mathcal{S}}_t}$. Then, on the target and selected auxiliary domains, we borrow the idea of the D-trace loss (Zhang and Zou, 2014) and estimate $\hat{\Delta}_t = \arg\min_{\Delta} \left(\frac{1}{2} \text{tr}\{\Delta^\top \Delta\} - \text{tr}\{(\hat{\Delta}_t^{(\check{k}_t)})^\top \Delta\} + \lambda_1 \|\Delta\|_1 \right)$, which essentially conducts an adaptive thresholding on $\hat{\Delta}_t^{(\check{k}_t)}$ and shrinks some of its small elements to be exactly 0 in $\hat{\Delta}_t$. With $\hat{\Delta}_t$, the estimate of $\Theta^{\hat{\mathcal{S}}_t}$ can be obtained as $\hat{\Theta}^{\hat{\mathcal{S}}_t} = \arg\min_{\Theta} \left(\frac{1}{2} \text{tr}\{\Theta^\top \hat{\Sigma}_{\hat{\mathcal{S}}_t}^{(\check{k}_t)} \Theta\} - \text{tr}\{(\hat{\Delta}_t^\top + \mathbf{I}_{|\hat{\mathcal{S}}_t|}) \Theta\} + \lambda_2 \|\Theta\|_{1, \text{off}} \right)$, where $\hat{\Sigma}_{\hat{\mathcal{S}}_t}^{(\check{k}_t)}$ is the sample covariance matrix of the selected auxiliary domain $\mathbf{X}^{(\check{k}_t)}$. This multi-step transfer learning method shares a similar spirit with Li et al. (2022b) albeit with some slight modifications. More details are provided in the Supplementary File.

Once $k_{j,t}^{no}$ is determined for each node j , $\hat{\mathcal{A}}_t$ can be estimated as

$$\hat{\mathcal{A}}_t = \left\{ j : \max_{l \in \hat{\mathcal{S}}_t \setminus \{j\}} n_{k_{j,t}^{no}} \hat{T} \left(\hat{e}_{j, \hat{\mathcal{S}}_t}^{(k_{j,t}^{no})}, x_l^{(k_{j,t}^{no})} \right) \leq (\Phi^{-1}(1 - \alpha_{k_{j,t}^{no}}/2))^2 \right\}, \quad (4.5)$$

where $\alpha_{k_{j,t}^{no}}$ is the significance level of the independence test. The independence test in (4.5) is exclusively based on the detected auxiliary DAG that shares exactly the same local structure as the target DAG, which can outperform the single DAG learning (Zhao et al., 2022) with a smaller sample size. In the proposed local structural transfer, the target domain is only used to efficiently detect informative structure-informative DAG via the well-designed criterion in (4.4), which shares an analogous spirit with bias correction using the target domain only in the parameter transfer procedure (Li et al., 2022a,b; Tian and Feng, 2022).

Remark 2. (Negative transfer) The developed method relies on the existence of structure-informative auxiliary domains. To safeguard the extreme case with no informative auxiliary domain, we can modify (4.4) by introducing a thresholding constant $\xi_{n,t}$, and declare a structure-informative auxiliary DAG only when the minimum in (4.4) is smaller than $\xi_{n,t}$. If no auxiliary DAG can be declared, we simply construct (4.5) based only on the target domain.

Remark 3. (Multiple informative auxiliary DAGs) By introducing $\xi_{n,t}$ as in Remark 2, we can declare multiple informative auxiliary DAGs for each node $j \in \hat{\mathcal{S}}_t$, whose indices are denoted as $\hat{\mathcal{K}}_{j,t}^N$. Then, we can modify (4.5) as

$$\hat{\mathcal{A}}_t = \left\{ j : \sum_{k \in \hat{\mathcal{K}}_{j,t}^N} I \left[\max_{l \in \hat{\mathcal{S}}_t \setminus \{j\}} n_k \hat{T}(\hat{\mathbf{e}}_{j,\hat{\mathcal{S}}_t}^{(k)}, \mathbf{x}_l^{(k)}) \leq (\Phi^{-1}(1 - \alpha_k/2))^2 \right] > |\hat{\mathcal{K}}_{j,t}^N|/2 \right\},$$

which is essentially a majority voting scheme. However, such a treatment is sensitive to the value of $\xi_{n,t}$, since an inappropriate $\xi_{n,t}$ may introduce non-informative auxiliary DAGs in the voting that will deteriorate the learning accuracy.

5 Theoretical properties

This section presents some theoretical properties of the proposed transfer learning method for DAG, including the exact DAG reconstruction consistency of $\hat{\mathcal{G}}_0$ and $\hat{\mathbf{B}}$ under the simple and realistic cases. Define $\tilde{n} = \min_{k \in [K]} n_k$, $d_t = \|\Theta^{S_t^*}\|_{0,\infty}$, $\gamma_{t,n} = pI(t=0) + \max\{|\mathcal{S}_t|, n\}I(t>0)$, $\gamma_{t,n_k}^{(k)} = pI(t=0) + \max\{|\mathcal{S}_t^{(k)}|, n_k\}I(t>0)$, and $\delta_{h_t} = (1 + h_t)(h_t \sqrt{\frac{\log \gamma_{t,n}}{n}} \wedge h_t^2)$. The following technical conditions are made.

Condition 1. Both $\|\Theta^*\|_{1,\infty}$ and $\|\Theta^{(k)*}\|_{1,\infty}$ are bounded, and there exists a constant C_1 , such that $1/C_1 \leq \psi_{\min}(\Sigma^*) \leq \psi_{\max}(\Sigma^*) \leq C_1$ and $1/C_1 \leq \psi_{\min}(\Sigma^{(k)*}) \leq \psi_{\max}(\Sigma^{(k)*}) \leq C_1$ for any $k \in [K]$. For any $j \in \mathcal{N}$ and $k \in [K]$, both ϵ_j/σ_j and $\epsilon_j^{(k)}/\sigma_j^{(k)}$ follow a sub-Gaussian distribution.

Condition 2. Denote $\mathcal{C}_{tj} = \{l \in \mathcal{S}_t : [\Theta^{\mathcal{S}_t^*}]_{jl} \neq 0\}$, $\mathcal{C}_{tj}^c = \mathcal{S}_t \setminus \mathcal{C}_{tj}$, and $\Sigma_{\mathcal{C}_{tj}\mathcal{C}_{tj}}^*$ the sub-matrix with rows and columns of Σ^* indexed by \mathcal{C}_{tj} and \mathcal{C}_{tj} , respectively. There exists some constant $C_2 \in (0, 1]$ such that $\max_{t \in \{0, \dots, T-1\}} \max_{j \in \mathcal{S}_t, e \in \mathcal{C}_{tj}^c} \|\Sigma_{e\mathcal{C}_{tj}}^* (\Sigma_{\mathcal{C}_{tj}\mathcal{C}_{tj}}^*)^{-1}\|_1 \leq 1 - C_2$ and $\max_{k \in \mathcal{K}_t^P} \max_{t \in \{0, \dots, T-1\}} \max_{j \in \mathcal{S}_t, e \in \mathcal{C}_{tj}^c} \|\Sigma_{e\mathcal{C}_{tj}}^{(k)*} (\Sigma_{\mathcal{C}_{tj}\mathcal{C}_{tj}}^{(k)*})^{-1}\|_1 \leq 1 - C_2$.

Condition 3. Let $T^{(k)}$ denote the number of layers in \mathcal{G}_k . For any $k \in [K]$ and $t \in [T^{(k)} - 1]$,

$$\max_{l \in \mathcal{S}_t^{(k)} \setminus \{j\}} \text{dcov}^2(e_{j, \mathcal{S}_t}^{(k)}, x_l^{(k)}) = \begin{cases} 0, & \text{if } j \in \mathcal{A}_t^{(k)}; \\ \rho_{k,t}^2, & \text{if } j \in \mathcal{S}_t^{(k)} \setminus \mathcal{A}_t^{(k)}, \end{cases}$$

where $\rho_{k,t}^2 \geq C \max\{(d_t^{(k)})^3 \sqrt{n_k^{-1} \log \gamma_{t,n_k}^{(k)}}, n_k^{-\eta}\}$ with $0 < \eta < \frac{1}{2}$, $d_t^{(k)} = \|\Theta^{\mathcal{S}_t^{(k)*}}\|_{0,\infty}$, and a sufficiently large constant C .

Condition 4. The parameter-informative set $\mathcal{K}_t^P = \{k : \|\Delta_{\mathcal{S}_t}^{(k)*}\|_{1,\infty} + \|(\Delta_{\mathcal{S}_t}^{(k)*})^\top\|_{1,\infty} \leq h_t\}$ is non-empty for any $t \in [T - 1]$ and $h_t \lesssim d_t \sqrt{\frac{\log \gamma_{t,n}}{n}} \lesssim 1$. Moreover, $\min_{\tilde{k} \notin \mathcal{K}_t^P} \|\Delta_{\mathcal{S}_t}^{(\tilde{k})*}\|_{1,\infty} \gg d_t \sqrt{\frac{\log \gamma_{t,n}}{n}}$.

Condition 1 prevents both Θ^* and $\Theta^{(k)*}$ from divergence and characterizes the noise distribution implying that $x_j / \sqrt{\Sigma_{jj}}$ also follows a sub-Gaussian distribution, which has been commonly employed in literature (Lam and Fan, 2009; Zhao et al., 2022). Condition 2 limits the correlation between the zero and non-zero elements in both Σ^* and $\Sigma^{(k)*}$. This is analogous to the popular irrepresentable condition required for many lasso-type methods (Ravikumar et al., 2011; Zhang and Zou, 2014; Liu and Luo, 2015). Condition 3 assures nodes in $\mathcal{A}_t^{(k)}$ and $\mathcal{S}_t^{(k)} \setminus \mathcal{A}_t^{(k)}$ can be discriminated via distance covariance on the auxiliary DAGs only. This condition only enforces the requirement on auxiliary domains rather than the target domain. We also remark that the term $(d_t^{(k)})^3$ in the lower bound of $\rho_{k,t}^2$ is analogous to the best existing results in the literature of single DAG learning (Zhao et al., 2022). Condition 4 assures that there exists at least one parameter-informative auxiliary domain for each topological layer, and the second half of the condition can be regarded as

the detectable condition of the informative auxiliary domains. Such detectable conditions have been widely used in the literature of transfer learning, although their actual form may vary under different models (Tian and Feng, 2022).

5.1 Global transfer in the naive case

We now establish asymptotic consistency in terms of exact DAG recovery in the naive case where \mathcal{G}_k 's in \mathcal{K}_0^P are also global structure-informative.

Lemma 1. (Consistency of $\{\hat{\mathcal{A}}_t\}_{t=0}^{T-1}$) *Suppose that $\max_{k \in [\mathcal{K}_0^P]} \frac{(d_0^{(k)})^6 \log p}{n_k} \lesssim 1$ and Conditions 1 to 4 hold, then there exist some positive constants c , C_α , and $\tau > 2$ such that*

$$\Pr(\hat{\mathcal{A}}_t = \mathcal{A}_t \text{ for any } t) \geq 1 - cp^{2-\tau} - cT\tilde{n}^{2-\tau} - cTp^2 \exp\{-c\tilde{n}^{(1-2\eta)/3}\},$$

provided that the significance level of the independence test in (4.3) is set as $\alpha_{\tilde{k}} = 2(1 - \Phi(C_\alpha \sqrt{n_{\tilde{k}} \rho_{\tilde{k},t}}))$.

Lemma 1 ensures that all topological layers $\{\mathcal{A}_t\}_{t=0}^{T-1}$ in \mathcal{G}_0 can be exactly recovered by the proposed transfer learning method with the help from the global structure-informative auxiliary DAG. The significance level $\alpha_{\tilde{k}}$ needs to be determined properly as in Kalisch and Bühlman (2007) and Zhao et al. (2022).

The consistency of reconstructing $\hat{\mathcal{G}}_0$ is then established following mathematical induction, leading to the asymptotic consistency in terms of exact DAG recovery.

Theorem 1. (Consistency of $\hat{\mathcal{G}}_0$ and $\hat{\mathbf{B}}$) *Suppose that all the conditions in Lemma 1 hold, $n_k \geq C(T^{1/(\tau-2)}(d_0^{(k)})^6 [\log(\max\{p, n_k\})]^{3/(1-2\eta)})$ for a sufficiently large constant C and $k \in \mathcal{K}_0^P$, and $\sqrt{\frac{\delta_{h_0}}{d_0}} + \sqrt{\frac{\log p}{\tilde{n}+n}} \lesssim \min_{(j,l) \in \{(j,l): \beta_{jl}^* \neq 0\}} |\beta_{jl}^*|$. It then holds true that $\Pr(\hat{\mathcal{G}}_0 = \mathcal{G}_0) \rightarrow 1$ as $n \rightarrow \infty$, and $\|\hat{\mathbf{B}} - \mathbf{B}^*\|_F = O_p\left(\sqrt{|\mathcal{E}_0| \frac{\delta_{h_0}}{d_0}} + |\mathcal{E}_0| \frac{\log p}{\tilde{n}+n}\right)$.*

Theorem 1 establishes the estimation consistency of $\widehat{\mathcal{G}}_0$ and $\widehat{\mathbf{B}}$ with global structure-informative auxiliary DAGs. For the target sample size, Theorem 1 hold true as long as $n \geq Cd_0^2 \log p$ in Condition 4, which is in sharp contrast to the single task DAG learning (Zhao et al., 2022), $n \geq C(T^{1/(\tau-4)}d_0^6[\log(\max\{p, n\})]^{3/(1-2\eta)})$. Moreover, when $\tilde{n} \gg n$ and $h_0 \ll d_0\sqrt{\frac{\log p}{n}}$, $\|\widehat{\mathbf{B}} - \mathbf{B}^*\|_F = O_p\left(\sqrt{|\mathcal{E}_0|\frac{\delta_{h_0}}{d_0} + |\mathcal{E}_0|\frac{\log p}{\tilde{n}+n}}\right)$ achieves a faster convergence rate than that using the target domain only, $O_p\left(\sqrt{|\mathcal{E}_0|\frac{\log p}{n}}\right)$. It is also interesting to note that the minimum signal of \mathbf{B}^* can be relaxed to $\sqrt{\frac{\delta_{h_0}}{d_0}} + \sqrt{\frac{\log p}{\tilde{n}+n}}$ from $\sqrt{\frac{\log p}{n}}$ using the target domain only.

5.2 Local transfer in the realistic case

We now turn to establishing the asymptotic exact DAG recovery via local transfer in the realistic case with node-level structure-informative auxiliary DAGs only. We start with the oracle setting with known node-level structure-informative auxiliary DAGs. Similar to Condition 4, the following Condition 5 assures the existence of node-level structure-informative auxiliary DAGs for each node j .

Condition 5. Let $\mathcal{K}_j^N = \{k : \mathcal{G}_k \text{ is node-}j \text{ structure-informative}\}$, then \mathcal{K}_j^N is non-empty for any $j \in \mathcal{S}_0$.

Lemma 2 provides an important benchmark, establishing the exact recovery of all the topological layers $\{\mathcal{A}_t\}_{t=0}^{T-1}$ in \mathcal{G}_0 in the oracle setting.

Lemma 2. Suppose that Conditions 1 to 5 hold. For $\widehat{\mathcal{A}}_t$ detected in (4.5) with the known node- j structure-informative \mathcal{G}_{k_j} for each j , there exist some positive constants c , C_α and $\tau > 2$ such that

$$\Pr(\widehat{\mathcal{A}}_t = \mathcal{A}_t, \text{ for any } t = 0, \dots, T-1) \geq 1 - cp^{2-\tau} - cT\tilde{n}^{2-\tau} - cTp^2 \exp\{-c\tilde{n}^{(1-2\eta)/3}\},$$

where the significance level in (4.5) is set as $\alpha_{k_j} = 2(1 - \Phi(C_\alpha \sqrt{n_{k_j}} \rho_{k_j,t}))$.

We then proceed to conduct an asymptotic analysis of the proposed detection method with unknown node-level structure-informative auxiliary DAGs. In this more challenging case, some additional conditions are necessary.

Condition 6. For any $t = 0, \dots, T - 1$,

$$\max_{l \in \mathcal{S}_t \setminus \{j\}} \text{dcov}^2(e_{j, \mathcal{S}_t}, x_l) = \begin{cases} 0, & \text{if } j \in \mathcal{A}_t; \\ \rho_{0,t}^2, & \text{if } j \in \mathcal{S}_t \setminus \mathcal{A}_t, \end{cases}$$

where $\rho_{0,t}^2 \geq C(\max\{d_t^{3/2}(\sqrt{\frac{\delta_{h_t}}{d_t}} + \sqrt{\frac{\log \gamma_{t,\tilde{n}}}{\tilde{n}+n}}), n^{-\eta}\})$ with $0 < \eta < \frac{1}{2}$ and a sufficiently large constant C .

Condition 7. For $j \in \mathcal{S}_0$, if $\tilde{k} \notin \mathcal{K}_j^N$, then $\max_{l' \in \mathcal{S}_{t_j} \setminus \{j\}} \text{dcov}^2(e_{j, \mathcal{S}_{t_j}}^{(\tilde{k})}, x_{l'}^{(\tilde{k})}) > \rho_{0,t_j}^2$; and for $j \in \mathcal{S}_0 \setminus \mathcal{A}_0$, there exists $k \in \mathcal{K}_j^N$ such that, $(1 - \kappa)\rho_{0,t}^2 < \max_{l \in \mathcal{S}_t \setminus \{j\}} \text{dcov}^2(e_{j, \mathcal{S}_t}^{(k)}, x_l^{(k)}) < (1 + \kappa)\rho_{0,t}^2$ for any $t < t_j$ and some constant $0 < \kappa < 1$.

Condition 6 prevents the distance covariance being too small in the target DAG to discriminate nodes in \mathcal{A}_t and $\mathcal{S}_t \setminus \mathcal{A}_t$. More interestingly, when $\tilde{n} \gg n$ and $h_t \ll d_t \sqrt{\frac{\log \gamma_{t,n}}{n}}$, the term $d_t^{3/2}(\sqrt{\frac{\delta_{h_t}}{d_t}} + \sqrt{\frac{\log \gamma_{t,\tilde{n}}}{\tilde{n}+n}})$ in Condition 6 can be substantially smaller than $d_t^3 \sqrt{\frac{\log \gamma_{t,n}}{n}}$ as in the single-task learning for DAG (Zhao et al., 2022). Condition 7, as the detectable condition of informative auxiliary domains, assures that informative auxiliary domains shall be sufficiently closer to the target domain than the non-informative auxiliary domain, so that the informative auxiliary domains can be efficiently detected. To verify Condition 7, encompassing a wide range of auxiliary DAG scenarios, is not an impractical endeavor. Indeed, a variety of intuitive examples are constructed in numerical simulations.

Theorem 2. (Consistency of $\hat{\mathcal{A}}_0$) When constructing \mathcal{A}_0 using (4.4), suppose all the conditions in Lemma 2 and Conditions 6 - 7 hold, and $\max_{k \in [K]} \frac{(d_0^{(k)})^6 \log p}{n_k} \lesssim 1$, then there

exist some positive constants c , C_α , and $\tau > 2$ such that

$$\text{pr}(\hat{\mathcal{A}}_0 = \mathcal{A}_0) \geq 1 - cp^{2-\tau} - cp \exp\{-cn^{(1-2\eta)/3}\} - cp^2 \exp\{-c\tilde{n}^{(1-2\eta)/3}\},$$

provided that the significance level of the independence test in (4.5) is set as $\alpha_k = 2(1 - \Phi(C_\alpha \sqrt{n_k} \rho_{k,0}))$ with $\rho_{k,0}$ defined in Condition 3 and $k = k_{j,0}^{no}$.

Theorem 2 ensures that the lowest layer \mathcal{A}_0 in \mathcal{G}_0 can be exactly recovered by the proposed transfer learning method with high probability. In the spirit of mathematical induction, the exact reconstruction of all the topological layers $\{\mathcal{A}_t\}_{t=0}^{T-1}$ can be guaranteed.

Corollary 1. (Consistency of $\{\hat{\mathcal{A}}_t\}_{t=0}^{T-1}$) Suppose that all the conditions in Theorem 2 hold, then there exist some positive constants c , C_α and $\tau > 2$ such that

$$\begin{aligned} \text{pr}(\hat{\mathcal{A}}_t = \mathcal{A}_t, \text{ for any } t = 0, \dots, T-1) \\ \geq 1 - cp^{2-\tau} - cTn^{2-\tau} - cTp \exp\{-cn^{(1-2\eta)/3}\} - cTp^2 \exp\{-c\tilde{n}^{(1-2\eta)/3}\}, \end{aligned}$$

provided that the significance level of the independence test in (4.5) is set as $\alpha_k = 2(1 - \Phi(C_\alpha \sqrt{n_k} \rho_{k,t}))$ with $\rho_{k,t}$ defined in Condition 3 and $k = k_{j,t}^{no}$.

After reconstructing all \mathcal{A}_t 's, we can also arrive at the consistency of $\hat{\mathcal{G}}_0$ with node-level structure-informative auxiliary DAGs.

Theorem 3. (Consistency of $\hat{\mathcal{G}}_0$ and $\hat{\mathbf{B}}$) Suppose that all the conditions in Corollary 1 hold, $n \geq C((T^{1/(\tau-2)} + d_0^3)[\log(\max\{p, n\})]^{3/(1-2\eta)})$, and $\sqrt{\frac{\delta_{h_0}}{d_0}} + \sqrt{\frac{\log p}{\tilde{n}+n}} \lesssim \min_{(j,l) \in \{(j,l): \beta_{jl}^* \neq 0\}} |\beta_{jl}^*|$. It then follows that

$$\text{pr}(\hat{\mathcal{G}}_0 = \mathcal{G}_0) \rightarrow 1 \text{ as } n \rightarrow \infty,$$

$$\text{and } \|\hat{\mathbf{B}} - \mathbf{B}^*\|_F = O_p\left(\sqrt{|\mathcal{E}_0| \frac{\delta_{h_0}}{d_0} + |\mathcal{E}_0| \frac{\log p}{\tilde{n}+n}}\right).$$

Theorem 3 establishes the asymptotic exact recovery of \mathcal{G}_0 and parameter estimation consistency for the linear non-Gaussian DAG, which holds true even for the high dimensional

case with $p = O(\exp(n^{c_\eta}/T^{c_\eta/(\tau-2)}))$ with $c_\eta = \frac{1-2\eta}{3}$. It is also important to remark that the proposed local transfer method by exploiting the node-level structure-informative auxiliary DAGs relaxes the sample complexity from $n \geq C(T^{1/(\tau-4)}d_0^6[\log(\max\{p, n\})]^{3/(1-2\eta)})$ (Zhao et al., 2022) to $n \geq C((T^{1/(\tau-2)} + d_0^3)[\log(\max\{p, n\})]^{3/(1-2\eta)})$. Moreover, similar to Theorem 1, the minimum signal condition on \mathbf{B}^* is relatively relaxed and the estimation error rate is improved when $\tilde{n} \gg n$ and $h_0 \ll d_0\sqrt{\frac{\log p}{n}}$.

Remark 4. *It is also interesting to compare the theoretical results for the simple and realistic cases. In terms of the condition and estimation error of \mathbf{B}^* , Theorem 3 for the realistic case matches up with the results in Theorem 1 for the naive case, indicating that the proposed method for the realistic case achieves desirable theoretical properties as if the global structure-informative auxiliary DAGs exist. Furthermore, from Lemma 1 for the naive case and Corollary 1 for the realistic case, the tail probability increases by $cTn^{2-\tau} + cTp \exp\{-cn^{(1-2\eta)/3}\}$ in the realistic case, which is the cost of searching for node-level structure-informative auxiliary DAGs for each node in each layer. Similar observations can also be observed from Lemma 2 for the oracle setting with known node-level structure-informative auxiliary DAGs and Corollary 1 for the realistic case. These comparisons demonstrate the effectiveness of the proposed method for recovering topological layers in the realistic case.*

Remark 5. *Although the theoretical results are established under the sub-Gaussian noise assumption, they can be generalized, with slight modification, to any noises satisfying the bounded moment condition that $\max_j E[(\epsilon_j/\sigma_j)^{4m}] \leq M$ for an integer $m > 1$ and a positive constant M .*

5.3 Further theoretical results and comparison

Note that the results in both Sections 5.1 and 5.2 assume the existence of a parameter-informative auxiliary DAG, which can be further relaxed with a slightly stronger signal.

Condition 8. For any $t = 0, \dots, T - 1$,

$$\max_{l \in \mathcal{S}_t \setminus \{j\}} d\text{cov}^2(e_{j, \mathcal{S}_t}, x_l) = \begin{cases} 0, & \text{if } j \in \mathcal{A}_t; \\ \rho_{0,t}^2, & \text{if } j \in \mathcal{S}_t \setminus \mathcal{A}_t, \end{cases}$$

where $\rho_{0,t}^2 \geq C(\max\{d_t^{3/2} \sqrt{\frac{\log \gamma_{t,n}}{n}}, n^{-\eta}\})$ and a sufficiently large constant C .

The following two corollaries demonstrate the theoretical improvement of the local structural transfer with $\hat{\Theta}^{\hat{\mathcal{S}}_t}$ estimated using the target domain only in the case where there are only node-level structure-informative auxiliary DAGs and no parameter-informative ones.

Corollary 2. (Consistency of $\{\hat{\mathcal{A}}_t\}_{t=0}^{T-1}$) Suppose that Conditions 1-3, 5, and 7-8 hold, then there exist some positive constants c , C_α and $\tau > 2$ such that

$$\begin{aligned} \text{pr}(\hat{\mathcal{A}}_t = \mathcal{A}_t, \text{ for any } t = 0, \dots, T - 1) \\ \geq 1 - cp^{2-\tau} - cTn^{2-\tau} - cTp^2 \exp\{-cn^{(1-2\eta)/3}\} - cTp^2 \exp\{-c\tilde{n}^{(1-2\eta)/3}\}. \end{aligned}$$

Corollary 3. (Consistency of $\hat{\mathcal{G}}_0$ and $\hat{\mathbf{B}}$) Suppose that all the conditions in Corollary 2 hold, $n \geq C((T^{1/(\tau-2)} + d_0^3)[\log(\max\{p, n\})]^{3/(1-2\eta)})$, and $\sqrt{\frac{\log p}{n}} \lesssim \min_{(j,l) \in \{(j,l): \beta_{jl}^* \neq 0\}} |\beta_{jl}^*|$. It then follows that $\text{pr}(\hat{\mathcal{G}}_0 = \mathcal{G}_0) \rightarrow 1$ as $n \rightarrow \infty$, and $\|\hat{\mathbf{B}} - \mathbf{B}^*\|_F = O_p\left(\sqrt{|\mathcal{E}_0| \frac{\log p}{n}}\right)$.

Table 1 summarizes the theoretical results and required conditions in different scenarios for a comprehensive comparison. Some interesting observations, with a focus on the scenario without parameter-informative auxiliary DAG, can be made.

- The estimation error of $\hat{\mathbf{B}}$ and the minimum signal of \mathbf{B}^* cannot be reduced using the local structure transfer method without parameter-informative auxiliary DAGs. This is rather expected as these improvements rely on the parameter transfer.
- The minimum signal condition on the distance covariance can be partially improved

Table 1: Theoretical comparisons of different scenarios, where P stands for parameter-informative, Global & Node stand for global or node-level structure-informative, and Single stands for single DAG learning with no auxiliary DAGs.

	minimum signal of \mathbf{B}	error of \mathbf{B}	† minimum signal of $\rho_{0,0}^2$	‡ tail probability of $\hat{\mathcal{A}}_t = \mathcal{A}_t$	target sample complexity
P+Global	$\sqrt{\frac{\delta_{h_0}}{d_0}} + \sqrt{\frac{\log p}{n+n}}$	$\sqrt{ \mathcal{E}_0 (\frac{\delta_{h_0}}{d_0} + \frac{\log p}{n+n})}$	None	$cp^{2-\tau} + cT\tilde{n}^{2-\tau} + cTp^2 \exp\{-c\tilde{n}^{c_\eta}\}$	$d_0^2 \log p$
P+Node	$\sqrt{\frac{\delta_{h_0}}{d_0}} + \sqrt{\frac{\log p}{n+n}}$	$\sqrt{ \mathcal{E}_0 (\frac{\delta_{h_0}}{d_0} + \frac{\log p}{n+n})}$	$d_0^{3/2}(\sqrt{\frac{\delta_{h_0}}{d_0}} + \sqrt{\frac{\log p}{n+n}})$	$cp^{2-\tau} + cTn^{2-\tau} + cTp \exp\{-cn^{c_\eta}\}$	$(T^{\frac{1}{\tau-2}} + d_0^3)[\log(\max\{p, n\})]^{\frac{1}{c_\eta}}$
Node	$\sqrt{\frac{\log p}{n}}$	$\sqrt{ \mathcal{E}_0 \sqrt{\frac{\log p}{n}}}$	$d_0^{3/2} \sqrt{\frac{\log p}{n}}$	$cp^{2-\tau} + cTn^{2-\tau} + cTp \exp\{-cn^{c_\eta}\}$	$(T^{\frac{1}{\tau-2}} + d_0^3)[\log(\max\{p, n\})]^{\frac{1}{c_\eta}}$
Single	$\sqrt{\frac{\log p}{n}}$	$\sqrt{ \mathcal{E}_0 \sqrt{\frac{\log p}{n}}}$	$d_0^3 \sqrt{\frac{\log p}{n}}$	$cp^{4-\tau} + cTn^{4-\tau} + cTp^2 \exp\{-cn^{c_\eta}\}$	$T^{\frac{1}{\tau-4}} d_0^6 [\log(\max\{p, n\})]^{\frac{1}{c_\eta}}$

† The common item $n^{-\eta}$ is omitted, and the comparison focuses on $t = 0$ for clearer comparison, and $\delta_{h_0} = (1 + h_0)(h_0 \sqrt{\frac{\log p}{n}} \wedge h_0^2)$ and $c_\eta = \frac{1-2\eta}{3} \in (0, \frac{1}{3})$.

‡ In both “P+Node” and “Node”, the term $cTp^2 \exp\{-c\tilde{n}^{c_\eta}\}$ dominated by others is omitted.

even without parameter-informative auxiliary DAGs. It is due to the fact that both parameter transfer and structure transfer can help relax this condition.

- Most importantly, the tail probability of $\hat{\mathcal{A}}_t = \mathcal{A}_t$ and the target sample complexity to ensure the consistency of $\hat{\mathcal{G}}_0$ can still be improved benefiting from structure-informative DAGs only, and its improved effectiveness is not affected by the presence of parameter-informative auxiliary DAGs. Specifically, the tail probability in the case of “Node” is much smaller than that of “Single”, in the high dimensional case with $p \gg [\exp(cn^{c_\eta})/T]^{1/\tau} + [\exp(cn^{c_\eta})/n^{\tau-2}]^{1/2}$, and the sample complexity is also substantially reduced with only the node-level structure-informative DAG.

6 Simulation study

This section examines the numerical performance of the proposed transfer DAG learning methods on two simulated examples. For each example, we consider both the simple and realistic cases for auxiliary DAGs, as described in Section 4.2. The DAG structures in both simulated examples are illustrated in Figures S1 and S2 of the Supplementary File.

Example 1. For the target DAG, we consider a sparse hub graph with $T = 2$, $\mathcal{A}_0 = \{4, \dots, p\}$, and $\mathcal{A}_1 = \{1, 2, 3\}$. For each node in \mathcal{A}_1 , we randomly select $\lceil (\log p)^2 \rceil$ nodes

in \mathcal{A}_0 as its children, and the coefficient of each directed edge is uniformly generated from $[-1.5, -0.5] \cup [0.5, 1.5]$.

For the naive case, three informative auxiliary DAGs are generated by randomly adding directed edges from each hub node in \mathcal{A}_1 to its non-child nodes in \mathcal{A}_0 in the target DAG with probability 0.1, and the coefficients of the added directed edges are uniformly generated from $[-\mu, \mu]$ with $\mu = 0.1\sqrt{\frac{\log p}{n}}$. Clearly, these auxiliary DAGs are both parameter-informative and global structure-informative. For the realistic case, the parameter-informative auxiliary DAG is generated based on the target DAG, by adding directed edges from half of the isolated nodes in \mathcal{A}_0 to other nodes with probability 0.5. The coefficients of the added directed edges are also uniformly generated from $[-\mu, \mu]$. Its structure is completely different from that of the target DAG, but their parameters are close. In addition, three node-level structure-informative DAGs are also generated, each with only one hub node selected from $\{1, 2, 3\}$. Furthermore, for each case, four non-informative auxiliary DAGs with hub nodes that are not in \mathcal{A}_1 are also generated.

Example 2. For the target DAG, we consider a DAG consisting of two equal-sized disjoint scale-free subgraphs. Each subgraph is generated by the Barabási-Albert (BA) model, where we start with a single node, and a node with 2 directed edges is added to the graph at each step. The coefficient of each directed edge is uniformly generated from $[-1.5, -0.5] \cup [0.5, 1.5]$.

For the naive case, two informative auxiliary DAGs are generated by randomly adding directed edges in the target DAG from nodes in \mathcal{A}_{t+1} of one subgraph to nodes in \mathcal{A}_t of the other subgraph for $t = 0, 1, \dots, T - 2$. The coefficients of the added directed edges are uniformly generated from $[-\mu, \mu]$. These steps generate the auxiliary DAGs with the same topological layers and similar parameters as the target DAG. For the realistic case, the parameter-informative auxiliary DAG is generated by randomly adding directed edges in the target DAG from nodes in one subgraph to nodes in the other subgraph with a probability

of 0.5, regardless of their topological layers. The coefficients of the added directed edges are uniformly generated from $[-\mu, \mu]$. We also consider two node-level structure-informative DAGs, each with the same subgraph as the target DAG, while the other subgraph is replaced by an arbitrary scale-free graph. Moreover, for each case, four non-informative auxiliary DAGs with arbitrary scale-free structures are generated.

In addition, we randomly generate ϵ_j 's from either uniform distribution $[-1 - 2j/p, 1 + 2j/p]$ for $j = 1, \dots, p$ or student t_9 distribution with variance $\sigma_j^2 = (2 + 4j)^2/12$, ensuring heteroskedasticity of the generated data. The target sample size and dimension are set as $(n, p) = (100, 100)$, and the auxiliary sample size is set to $\tilde{n} = \omega n$ with $\omega \in \{3, 4, 5\}$.

We compare our method with some popular linear non-Gaussian single DAG learning methods, such as the topological layer-based learning algorithm (TL; Zhao et al., 2022), the direct high-dimension learning algorithm (MDirect; Wang and Drton, 2020), and the pairwise learning algorithm (Pairwise; Hyvärinen and Smith, 2013); some general single DAG learning methods, including the high dimensional constraint-based PC algorithm (PC; Kalisch and Bühlman, 2007) and a hybrid version of max-min hill-climbing algorithm (MMHC; Tsamardinos et al., 2006); and a multi-task learning method of DAGs (jointDAG; Wang et al., 2020). The proposed methods described in Sections 4.1 and 4.2 are denoted as Global-Trans and Local-Trans, respectively. The simple and realistic cases of auxiliary DAGs are denoted as “Aux1” and “Aux2”, respectively. The significance level of independent tests in our methods, TL and PC is set as $\alpha = 0.01$ following the same treatment as in Kalisch and Bühlman (2007).

The performances of all the competing methods are measured by several metrics. The true positive rate (TPR), false discovery rate (FDR), and F1-score measure the accuracy of estimated directed edges. The normalized structural Hamming distance (HM; Tsamardinos et al., 2006), measuring the smallest number of edge insertions, deletions, and flips needed to convert the estimated DAG into the true one, and Matthews correlation coefficient (MCC;

Yuan et al., 2019) are employed to evaluate the similarity between the estimated and true DAGs. Moreover, the relative error between $\hat{\mathbf{B}}$ and \mathbf{B}^* , $\text{re}(\hat{\mathbf{B}}) = \|\hat{\mathbf{B}} - \mathbf{B}^*\|_F / \|\mathbf{B}^*\|_F$, is also reported. Note that a good estimation is implied with small values of FDR, HM, and $\text{re}(\hat{\mathbf{B}})$, but large values of TPR, F1-score, and MCC.

The averaged metrics over 100 independent replications under uniform distributed residuals are summarized in Tables 2 and 3, whereas more numerical results are provided in Tables S1 and S2 in the Supplementary File. Observations made are very similar under different settings.

Table 2: Averaged metrics and their standard deviation in parenthesis for Example 1 with uniform distributed residuals

			Recall	FDR	F1-score	MCC	HM	$\text{re}(\hat{\mathbf{B}})$
		MMHC	0.0567(0.0272)	0.9639(0.0176)	0.0441(0.0213)	0.0380(0.0220)	0.0149(0.0007)	1.0622(0.0192)
		PC	0.0575(0.0250)	0.9126(0.0371)	0.0692(0.0295)	0.0663(0.0302)	0.0093(0.0005)	1.0122(0.0181)
		Pairwise	0.4227(0.2213)	0.8304(0.0910)	0.2411(0.1276)	0.2603(0.1418)	0.0163(0.0035)	0.8544(0.1172)
		MDirect	0.0305(0.0336)	0.9915(0.0094)	0.0132(0.0145)	0.0046(0.0178)	0.0231(0.0065)	1.5507(0.0019)
		TL	0.9253(0.0391)	0.1436(0.0482)	0.8887(0.0344)	0.8891(0.0343)	0.0014(0.0004)	0.2836(0.0612)
JointDAG	Aux1	$\omega = 3$	0.8333(0.2887)	0.2176(0.0713)	0.7966(0.1847)	0.7737(0.2041)	0.0593(0.0449)	1.2667(0.0480)
		$\omega = 4$	0.9048(0.1091)	0.2414(0.0682)	0.8251(0.0858)	0.7983(0.1025)	0.0593(0.0280)	1.2329(0.0832)
		$\omega = 5$	0.9286(0.1237)	0.2473(0.1226)	0.8313(0.1245)	0.8064(0.1475)	0.0593(0.0449)	1.1752(0.2433)
	Aux2	$\omega = 3$	0.8571(0.0714)	0.2333(0.0688)	0.8092(0.0685)	0.7778(0.0808)	0.0630(0.0231)	1.3283(0.1061)
		$\omega = 4$	0.9048(0.1650)	0.2281(0.0549)	0.8308(0.1019)	0.8068(0.1214)	0.0556(0.0294)	1.3056(0.0266)
		$\omega = 5$	0.9286(0.0714)	0.2636(0.0607)	0.8212(0.0643)	0.7957(0.0769)	0.0630(0.0231)	1.2521(0.0672)
	Global-Trans	$\omega = 3$	0.9937(0.0136)	0.0166(0.0185)	0.9884(0.0140)	0.9884(0.0141)	0.0001(0.0002)	0.0942(0.0398)
		$\omega = 4$	0.9970(0.0083)	0.0101(0.0131)	0.9934(0.0093)	0.9934(0.0093)	0.0001(0.0001)	0.0740(0.0322)
		$\omega = 5$	0.9963(0.0087)	0.0072(0.0122)	0.9945(0.0098)	0.9945(0.0099)	0.0001(0.0001)	0.0658(0.0276)
Local-Trans	Aux1	$\omega = 3$	0.9435(0.0354)	0.1642(0.0716)	0.8853(0.0519)	0.8867(0.0506)	0.0015(0.0007)	0.2049(0.0702)
		$\omega = 4$	0.9473(0.0371)	0.1545(0.0682)	0.8924(0.0491)	0.8937(0.0479)	0.0014(0.0007)	0.1936(0.0760)
		$\omega = 5$	0.9533(0.0374)	0.1290(0.0604)	0.9094(0.0443)	0.9102(0.0436)	0.0012(0.0006)	0.1770(0.0781)
	Aux2	$\omega = 3$	0.9243(0.1357)	0.0685(0.0387)	0.9227(0.0831)	0.9249(0.0795)	0.0009(0.0009)	0.2120(0.1813)
		$\omega = 4$	0.9408(0.1221)	0.0343(0.0246)	0.9489(0.0745)	0.9508(0.0702)	0.0006(0.0008)	0.1669(0.1742)
		$\omega = 5$	0.9658(0.0939)	0.0175(0.0332)	0.9720(0.0628)	0.9729(0.0600)	0.0003(0.0007)	0.1169(0.1354)
	Aux1	$\omega = 3$	0.8905(0.1738)	0.0676(0.0383)	0.9004(0.1108)	0.9053(0.1006)	0.0011(0.0010)	0.2586(0.2233)
		$\omega = 4$	0.9140(0.1644)	0.0349(0.0242)	0.9294(0.1075)	0.9340(0.0957)	0.0007(0.0010)	0.2032(0.2163)
		$\omega = 5$	0.9327(0.1495)	0.0199(0.0340)	0.9484(0.1050)	0.9520(0.0935)	0.0005(0.0009)	0.1665(0.2036)

The proposed transfer DAG learning method achieves a significant improvement in all metrics compared with its single-task and multi-task competitors, especially in Example 2. The improvement increases as the auxiliary sample size increases. Specifically, Global-Trans outperforms all other competitors in the “Aux1” case as expected, thanks to the strong information from the global structure-informative auxiliary DAG. Local-Trans, although

Table 3: Averaged metrics and their standard deviation in parenthesis for Example 2 with uniform distributed residuals

			Recall	FDR	F1-score	MCC	HM	re($\widehat{\mathbf{B}}$)
		MMHC	0.3728(0.0155)	0.2915(0.0316)	0.4885(0.0198)	0.5074(0.0213)	0.0153(0.0006)	0.8169(0.0218)
		PC	0.3107(0.0352)	0.3738(0.0665)	0.4152(0.0457)	0.4337(0.0486)	0.0171(0.0013)	0.8601(0.0367)
		Pairwise	0.8068(0.0841)	0.7002(0.0491)	0.4366(0.0642)	0.4766(0.0680)	0.0413(0.0070)	0.5833(0.1047)
		MDirect	0.0287(0.0139)	0.9821(0.0081)	0.0216(0.0095)	0.0024(0.0108)	0.0463(0.0140)	1.2071(0.0105)
		TL	0.5324(0.0351)	0.2045(0.0340)	0.6370(0.0288)	0.6449(0.0275)	0.0119(0.0008)	0.9769(0.0934)
JointDAG	Aux1	$\omega = 3$	0.5429(0.3113)	0.2786(0.0749)	0.6102(0.1862)	0.5275(0.2025)	0.0926(0.0421)	1.2238(0.0752)
		$\omega = 4$	0.6095(0.1091)	0.2042(0.0953)	0.6997(0.0858)	0.66687(0.0992)	0.0630(0.0280)	1.2227(0.0754)
		$\omega = 5$	0.6333(0.1487)	0.1933(0.1117)	0.7022(0.0856)	0.6864(0.1016)	0.0593(0.0280)	1.2116(0.1261)
	Aux2	$\omega = 3$	0.5143(0.1237)	0.3004(0.0538)	0.6031(0.0663)	0.5573(0.0770)	0.0926(0.0170)	1.1254(0.1141)
		$\omega = 4$	0.5542(0.1187)	0.2597(0.0566)	0.6395(0.0475)	0.5803(0.0428)	0.0852(0.0064)	1.1337(0.1937)
		$\omega = 5$	0.6571(0.1172)	0.1992(0.1091)	0.7185(0.0305)	0.6948(0.0393)	0.0593(0.0128)	1.0459(0.2354)
Global-Trans	Aux1	$\omega = 3$	0.7179(0.0355)	0.0687(0.0172)	0.8102(0.0219)	0.8144(0.0200)	0.0066(0.0006)	0.5735(0.0449)
		$\omega = 4$	0.7252(0.0290)	0.0617(0.0154)	0.8177(0.0198)	0.8218(0.0186)	0.0063(0.0006)	0.5590(0.0331)
		$\omega = 5$	0.7363(0.0211)	0.0593(0.0135)	0.8258(0.0142)	0.8293(0.0135)	0.0061(0.0004)	0.5428(0.0297)
	Aux2	$\omega = 3$	0.5107(0.0359)	0.2266(0.0318)	0.6144(0.0297)	0.6223(0.0280)	0.0125(0.0008)	0.9919(0.0703)
		$\omega = 4$	0.5503(0.0369)	0.2176(0.0310)	0.6451(0.0275)	0.6501(0.0256)	0.0118(0.0007)	0.9868(0.0755)
		$\omega = 5$	0.5773(0.0418)	0.2164(0.0280)	0.6639(0.0313)	0.6667(0.0294)	0.0114(0.0009)	0.9508(0.0819)
Local-Trans	Aux1	$\omega = 3$	0.7842(0.0371)	0.1941(0.0346)	0.7947(0.0333)	0.7909(0.0339)	0.0079(0.0013)	0.6370(0.0640)
		$\omega = 4$	0.8057(0.0414)	0.1706(0.0324)	0.8172(0.0352)	0.8138(0.0357)	0.0071(0.0013)	0.5981(0.0654)
		$\omega = 5$	0.8114(0.0387)	0.1613(0.0351)	0.8246(0.0346)	0.8215(0.0352)	0.0068(0.0013)	0.5871(0.0663)
	Aux2	$\omega = 3$	0.7858(0.0377)	0.1946(0.0347)	0.7951(0.0326)	0.7914(0.0332)	0.0079(0.0013)	0.6391(0.0661)
		$\omega = 4$	0.7861(0.0561)	0.1759(0.0369)	0.8041(0.0447)	0.8008(0.0446)	0.0075(0.0015)	0.6216(0.0763)
		$\omega = 5$	0.7961(0.0477)	0.1697(0.0411)	0.8126(0.0419)	0.8093(0.0426)	0.0072(0.0016)	0.6096(0.0868)

slightly inferior to Global-Trans, still dominates all the single-task learning methods. In the “Aux2” case without global structure-informative auxiliary DAGs, the performance of Global-Trans is not satisfactory and even worse than the single-task learning method TL, leading to the so-called “negative transfer” phenomenon. In sharp contrast, Local-Trans still outperforms all other methods in this complex and challenging setting with only node-level structure-informative auxiliary DAGs.

7 ADHD brain networks

Attention deficit hyperactivity disorder (ADHD) is a child-onset disorder of neurodevelopmental origins, which is related to anomalies of brain functional connectivities but its neural substrates and exact etiological bases are far from being fully understood. Unlike undirected network analysis, detecting causal relationships helps to discover directional regulatory effects between brain regions, which can enable researchers to gain a deeper understanding of

the ADHD neural etiology (Agoalikum et al., 2023). In this section, we apply the proposed transfer DAG learning method to study directed functional connectivity behaviors among brain regions in ADHD across multiple datasets, which is available at the ADHD-200 preprocessed repository (<http://neurobureau.projects.nitrc.org/ADHD200/Data.html>, Bellec et al., 2017). This dataset is collected from seven sites, each of which contains two groups consisting of typically developing controls (TDC) and ADHD. The detailed description of seven sites is summarized in Table S3 of the Supplementary File. The brain images are preprocessed following the standard Athena pipeline (Bellec et al., 2017) and parcellated into 116 regions of interest (ROIs) following the Anatomical Automatic Labeling (AAL) atlas.

We select the OHSU site as the target domain to further demonstrate the performance of the proposed method by performing a more in-depth biological exploration. The detected brain DAGs of TDC and ADHD have six and five topological layers, respectively, which are substantially different. To scrutinize their differences, the differential DAGs between TDC and ADHD groups are plotted in Figure 3, in which ROIs are labeled as the SRI24 code, and a cross-reference between the SRI24 code and full names of ROIs can be found in Table S4 of Supplementary File.

It is evident that the connection structures of TDC and ADHD patients are significantly different in the amygdala region labeled as 41 and 42. Specifically, it can be observed that the amygdala is a transition region in the ADHD patient, which receives more regulatory effects from the pallidum labeled as 75 and 76 compared to the TDC patient. In fact, the amygdala is involved in emotional regulation, especially negative emotions, and the activation of the amygdala caused by the pallidum may reflect emotional impairment in ADHD patients (Bonnet et al., 2015). On the other hand, the amygdala can project more regulatory effects to other regions such as the insula region labeled as 29 and 30, which is consistent with previous studies (Agoalikum et al., 2023). More regulatory effects can be observed from the frontal gyrus regions labeled as 3 to 16 to the cerebellum labeled as

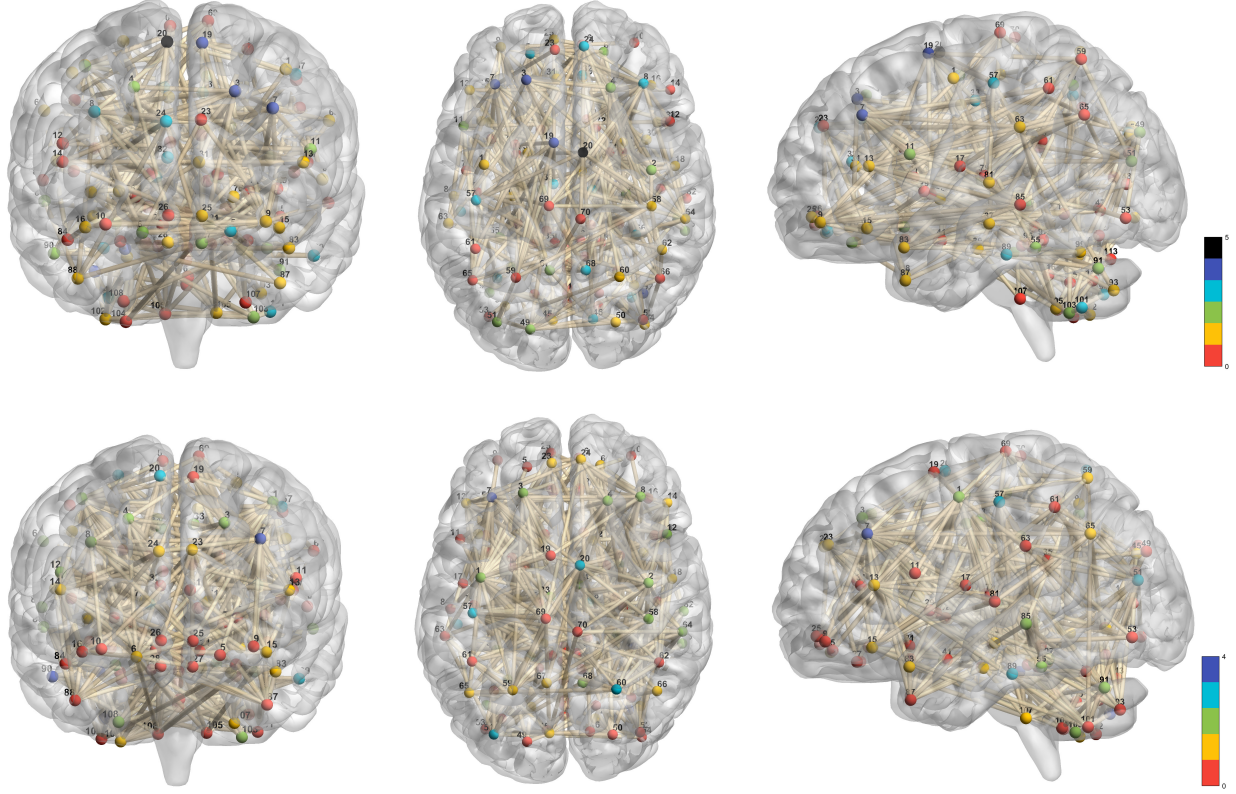


Figure 3: The differential DAGs of brain functional connectivity between ADHD and TDC groups. The top rows show the edges in TDC but not ADHD, whereas the bottom rows show the edges in ADHD but not TDC. In each row, three different views, coronal (left), axial (middle), and sagittal (right), are provided. Different topological layers in TDC and ADHD are distinguished by colors in top and bottom rows, respectively. The directionality of edges is naturally determined from higher to lower layers.

91 to 118 in the ADHD patient, which suggests frontal-cerebellum connectivity mechanism reported in existing ADHD studies (Giedd et al., 2001) and further provides evidence of the cerebellum involved ADHD pathophysiology. Actually, cerebellum abnormalities, especially in the structural and functional connectivity, have been reported in patients with ADHD (Tomasi and Volkow, 2012). Moreover, the superior frontal gyrus labeled as 25 and 26 and the inferior occipital gyrus labeled as 53 and 54, have more regulatory effects to other regions in TDC, which are consistent with existing findings that there is a decrease in functional connections between the superior frontal gyrus and other brain regions in ADHD, and that

inattention improvement is related to increased intrinsic brain activity in inferior occipital gyrus (Zhang et al., 2020), respectively.

8 Discussion

This paper proposes a transfer DAG learning framework, which is able to accommodate informative auxiliary DAGs with different levels of similarities. A novel set of structure similarity measures are also proposed to quantify the global or local similarity between the target and auxiliary DAGs. The substantial theoretical and numerical improvement of the proposed transfer DAG learning in terms of DAG reconstruction in the target study have been demonstrated. The proposed transfer learning framework can be extended to other structured graphical models, including Gaussian graphical model and Gaussian DAG model. Moreover, it is of interest to explore potential remedial treatment for possible negative transfer in the extreme case with no node-level structure-informative auxiliary DAGs.

References

- Agoalikum, E., Klugah-Brown, B., Hongzhou, W., Hu, P., Jing, J., and Biswal, B. B. (2023), “Structural differences among children, adolescents, and adults with attention deficit hyperactivity disorder and abnormal granger causality of the right pallidum and whole-brain,” *Frontiers in Human Neuroscience*, 17, 40.
- Bellec, P., Chu, C., Chouinard-Decorte, F., Benhajali, Y., Margulies, D. S., and Craddock, R. C. (2017), “The neuro bureau ADHD-200 preprocessed repository,” *Neuroimage*, 144, 275–286.
- Bonnet, L., Comte, A., Tatu, L., Millot, J.-L., Moulin, T., and Medeiros de Bustos, E.

- (2015), “The role of the amygdala in the perception of positive emotions: an “intensity detector”,” *Frontiers in Behavioral Neuroscience*, 9, 178.
- Cai, T. T. and Wei, H. (2021), “Transfer learning for nonparametric classification: Minimax rate and adaptive classifier,” *The Annals of Statistics*, 49, 100–128.
- Chen, W., Drton, M., and Wang, Y. S. (2019), “On causal discovery with an equal-variance assumption,” *Biometrika*, 106, 973–980.
- Chen, X., Sun, H., Ellington, C., Xing, E., and Song, L. (2021), “Multi-task learning of order-consistent causal graphs,” *Advances in Neural Information Processing Systems*, 34, 11083–11095.
- Danks, D., Glymour, C., and Tillman, R. (2008), “Integrating locally learned causal structures with overlapping variables,” *Advances in Neural Information Processing Systems*, 21.
- Ghoshal, A. and Honorio, J. (2018), “Learning linear structural equation models in polynomial time and sample complexity,” in *International Conference on Artificial Intelligence and Statistics*, PMLR.
- Giedd, J. N., Blumenthal, J., Molloy, E., and Castellanos, F. X. (2001), “Brain imaging of attention deficit/hyperactivity disorder,” *Annals of the New York Academy of Sciences*, 931, 33–49.
- Huang, B., Zhang, K., Gong, M., and Glymour, C. (2020), “Causal discovery from multiple data sets with non-identical variable sets,” in *Proceedings of the AAAI conference on artificial intelligence*, volume 34.
- Hyvärinen, A. and Smith, S. M. (2013), “Pairwise likelihood ratios for estimation of non-

- Gaussian structural equation models,” *The Journal of Machine Learning Research*, 14, 111–152.
- Kalisch, M. and Bühlman, P. (2007), “Estimating high-dimensional directed acyclic graphs with the PC-algorithm.” *Journal of Machine Learning Research*, 8.
- Lam, C. and Fan, J. (2009), “Sparsistency and rates of convergence in large covariance matrix estimation,” *The Annals of Statistics*, 37, 4254–4278.
- Li, S., Cai, T., and Duan, R. (2023b), “Targeting underrepresented populations in precision medicine: A federated transfer learning approach,” *The Annals of Applied Statistics*, 1–25.
- Li, S., Cai, T. T., and Li, H. (2022a), “Transfer learning for high-dimensional linear regression: Prediction, estimation, and minimax optimality,” *Journal of the Royal Statistical Society: Series B (Statistical Methodology)*, 1–26.
- (2022b), “Transfer learning in large-scale gaussian graphical models with false discovery rate control,” *Journal of the American Statistical Association*, 1–13.
- Li, S., Zhang, L., Cai, T. T., and Li, H. (2023a), “Estimation and inference for high-dimensional generalized linear models with knowledge transfer,” *Journal of the American Statistical Association*, 1–12.
- Liu, J., Sun, W., and Liu, Y. (2019), “Joint skeleton estimation of multiple directed acyclic graphs for heterogeneous population,” *Biometrics*, 75, 36–47.
- Liu, W. and Luo, X. (2015), “Fast and adaptive sparse precision matrix estimation in high dimensions,” *Journal of Multivariate Analysis*, 135, 153–162.
- Mooij, J. M., Magliacane, S., and Claassen, T. (2020), “Joint causal inference from multiple contexts,” *The Journal of Machine Learning Research*, 21, 3919–4026.

- Park, G. (2020), “Identifiability of additive noise models using conditional variances,” *The Journal of Machine Learning Research*, 21, 2896–2929.
- Peters, J. and Bühlmann, P. (2014), “Identifiability of Gaussian structural equation models with equal error variances,” *Biometrika*, 101, 219–228.
- Ravikumar, P., Wainwright, M. J., Raskutti, G., and Yu, B. (2011), “High-dimensional covariance estimation by minimizing ℓ_1 -penalized log-determinant divergence,” *Electronic Journal of Statistics*, 5, 935–980.
- Reeve, H. W., Cannings, T. I., and Samworth, R. J. (2021), “Adaptive transfer learning,” *The Annals of Statistics*, 49, 3618–3649.
- Shimizu, S. (2012), “Joint estimation of linear non-Gaussian acyclic models,” *Neurocomputing*, 81, 104–107.
- Shimizu, S., Hoyer, P. O., Hyvärinen, A., Kerminen, A., and Jordan, M. (2006), “A linear non-Gaussian acyclic model for causal discovery,” *Journal of Machine Learning Research*, 7.
- Spirtes, P., Glymour, C. N., Scheines, R., and Heckerman, D. (2000), *Causation, prediction, and search.*, MIT press.
- Székely, G. J., Rizzo, M. L., and Bakirov, N. K. (2007), “Measuring and testing dependence by correlation of distances,” *The Annals of Statistics*, 35, 2769–2794.
- Tian, Y. and Feng, Y. (2022), “Transfer learning under high-dimensional generalized linear models,” *Journal of the American Statistical Association*, 1–30.
- Tomasi, D. and Volkow, N. D. (2012), “Abnormal functional connectivity in children with attention-deficit/hyperactivity disorder,” *Biological Psychiatry*, 71, 443–450.

- Triantafillou, S. and Tsamardinos, I. (2015), “Constraint-based causal discovery from multiple interventions over overlapping variable sets,” *The Journal of Machine Learning Research*, 16, 2147–2205.
- Tsamardinos, I., Brown, L. E., and Aliferis, C. F. (2006), “The max-min hill-climbing Bayesian network structure learning algorithm,” *Machine learning*, 65, 31–78.
- Wang, Y., Segarra, S., and Uhler, C. (2020), “High-dimensional joint estimation of multiple directed Gaussian graphical models,” *Electronic Journal of Statistics*, 14, 2439 – 2483.
- Wang, Y. S. and Drton, M. (2020), “High-dimensional causal discovery under non-Gaussianity,” *Biometrika*, 107, 41–59.
- Yuan, Y., Shen, X., Pan, W., and Wang, Z. (2019), “Constrained likelihood for reconstructing a directed acyclic Gaussian graph,” *Biometrika*, 106, 109–125.
- Zhang, H., Zhao, Y., Cao, W., Cui, D., Jiao, Q., Lu, W., Li, H., and Qiu, J. (2020), “Aberrant functional connectivity in resting state networks of ADHD patients revealed by independent component analysis,” *BMC neuroscience*, 21, 1–11.
- Zhang, T. and Zou, H. (2014), “Sparse precision matrix estimation via lasso penalized D-trace loss,” *Biometrika*, 101, 103–120.
- Zhao, R., He, X., and Wang, J. (2022), “Learning linear non-Gaussian directed acyclic graph with diverging number of nodes,” *Journal of Machine Learning Research*, 23, 1–34.
- Zhuang, F., Qi, Z., Duan, K., Xi, D., Zhu, Y., Zhu, H., Xiong, H., and He, Q. (2020), “A comprehensive survey on transfer learning,” *Proceedings of the IEEE*, 109, 43–76.